8
Computer simulations of explosive volcanic eruptions

Kenneth H. Wohletz and Greg A. Valentine
Earth and Environmental Sciences Division,
Los Alamos National Laboratory,
Los Alamos, NM 87545, USA

Abstract

Today's large, high-speed computers provide the capability for the solution of the full set of two-phase, compressible Navier–Stokes equations in two or three dimensions. We have adapted computer codes that provide such solutions in order to study explosive volcanic phenomena. At present these fully non-linear conservation equations are cast in two-dimensional cylindrical coordinates, which, with closure equations, comprise 16 equations with 16 unknown variables. Solutions for several hundred seconds of simulated eruption time require 2–3 h of Cray-1 computer time. Over 100 simulations have been run to simulate the physics of highly unsteady blasts, sustained and steady Plinian eruptions, fountaining column eruptions, and multiphase flow of magma in lithospheric conduits. The calculations of unsteady flow show resemblance to shock-tube physics with propagation of shock waves into the atmosphere and rarefaction waves down the volcanic conduit. Simulations of steady-flow eruption demonstrate the importance of supersonic flow and overpressure of erupted jets of tephra and gases in determining whether the jet will buoyantly rise or collapse back to the Earth as a fountain. Flow conditions within conduits rising through the lithosphere determine eruptive conditions of overpressure, velocity, bulk density and vent size. Such conditions within conduit systems are thought to be linked to low-frequency, sustained seismicity known as volcanic tremor. These calculations demonstrate the validity of some analytical eruption calculations under limited conditions. In general though, the simulations show that consideration of non-linearities inherent in multiphase properties, compressibility and multiple dimensions lead to solutions that may greatly vary from simple, one-dimensional analytical approaches and often produce results not available to intuitive reasoning.

Contents

Magma Transport and Storage. Edited by M.P. Ryan

Notation

		Units
I_g	gas specific energy	J kg^{-1}
I_s	solid specific energy	J kg^{-1}
J	mass exchange rate	kg m^{-3} s^{-1}
J_e	energy source of mass exchange and phase change	J m^{-3} s^{-1}
K_g	momentum exchange, particles to gas	N m^{-3}
K_s	momentum exchange, gas to particles	N m^{-3}
K_p	ratio of exit pressure to atmospheric pressure	
M	Mach number	
R_g	heat exchange, particles to gas	J m^{-3} s^{-1}
R_s	heat exchange, gas to particles	J m^{-3} s^{-1}
Ri_m	Richardson number	
T_0	atmospheric temperature	K
T_{gm}	Thermogravitational parameter	
U_s	shock speed	m s^{-1}
c	sound speed	m s^{-1}
c_0	atmospheric sound speed	m s^{-1}
$\mathbf{g}$	gravitational acceleration	m s^{-2}
p	pressure	Pa
p_0	atmospheric pressure	Pa
p_1	chamber pressure	Pa
p_2	shocked pressure of atmosphere	Pa
r	spatial coordinate in radial direction	
t	time	s
$\mathbf{u}_g$	gas velocity vector	m s^{-1}
$\mathbf{u}_s$	solid velocity vector	m s^{-1}
u	radial velocity	m s^{-1}
v	vertical velocity	m s^{-1}
x	linear spatial coordinate	
y	shock strength	
z	spatial coordinate in vertical direction	
$\Delta\mathbf{u}$	$\mathbf{u}_g - \mathbf{u}_s$	m s^{-1}
γ	gas isentropic exponent	
ρ	density	kg m^{-3}
ρ_g	gas microscopic density	kg m^{-3}
ρ_s	solid microscopic density	kg m^{-3}
ρ_0	atmospheric density	kg m^{-3}
μ	limit of isentropic expansion	
θ_g	gas volume fraction	
θ_s	solids volume fraction	
τ	stress tensor	
ν_e	eddy viscosity	m^2 s^{-1}

Introduction

Computers have played an increasing role in geosciences over the last several decades in a variety of capacities, including managing data bases, digital mapping, geophysical data inversion, statistical analysis, and the modeling or simulation of physical and chemical processes, to name but a few. We discuss one of the newer applications, simulation based upon the solution of sets of differential equations that model the fundamental physical relationships of fluid mechanics. Historically, computers, especially those now called 'supercomputers', were developed because of the vision of John von Neumann (von Neumann and Richtmeyer, 1949; Ulam, 1980), who believed that all the necessary fundamental physical behavior of fluids could be expressed accurately by mathematical relationships. Von Neumann realized that the intrinsic non-linearity of these systems of differential equations and the large number of variables involved precluded analytical solution. He showed that the mathematical techniques of finite differences could provide very precise solutions to individual equations, but that to perform such calculations would be practically impossible without the utilization of machines that could rapidly process the billions of arithmetic steps required. Today we have those fast, large-memory machines, and the continued evolution of these computers promises to achieve Von Neumann's vision.

Explosive volcanism plays an important role in today's understanding of geodynamic relationships. It represents the high-flux end member of mass and energy transport through the Earth's lithosphere and is a major contributor to the chemical budget of the atmosphere. There is a growing understanding of the relationship of explosive volcanism to the chemical and physical character of the lithosphere and features of mantle dynamics. All of these interact in a strongly coupled system.

Our present capability of computer simulations of explosive volcanic eruptions has developed over the last decade through the stimuli of research programs at Los Alamos focused on understanding geothermal systems developed in calderas, modest efforts at characterizing and pre-

dicting volcanic hazards, and a large effort to bring the power of computational physics into the realm of earth sciences. This latter effort has followed a general, whole-Earth approach in which the large-scale behavior and character of the Earth's core and mantle, plate and atmospheric dynamics, and fluid migration within the lithosphere are viewed as a coupled system. It is our hope that by gaining an ability to confidently simulate the visible aspects of explosive eruptions, we can constrain some part of the lithospheric system through which magma migration occurs.

The following description of our explosive volcanism simulations will briefly review some geologic phenomena we attempt to model, the modeling approach we have adapted from other fields of computational physics, and the results of simulations for end-member types of explosive behavior, including unsteady or 'blast' eruptions, steady flows producing high standing tephra columns, eruptive 'fountains', and finally our ongoing research into the character of flow in subsurface conduits.

Explosive volcanic phenomena

Explosive eruptive phenomena are highly variable, because of the large number of thermodynamic, chemical, and physical behaviors of magma and the solid rocks through which it erupts. These phenomena have been classified by volcanologists by their overall eruptive features and their type-locality (MacDonald, 1972; Walker, 1973). From a physical point of view, the classification can be simplified further by a consideration of the general fluid dynamical flow regime within which various eruptions are thought to behave (e.g., Wilson, 1980). The major constituents of eruptive products are the solid materials, called tephra (pumice, ash and rock fragments) and gases (dominantly steam and carbon dioxide).

Figure 1 shows the 22 July 1980 eruption cloud of Mount St Helens. The mushroom-shaped top of the cloud is convectively rising to a height of about 15 km above the vent. Several features of the eruptive phenomena portrayed are generally common to most explosive eruptions. The cloud shows bulbous, swirling eddies, which are evidence of turbulence, and their average diameter of about 10–100 m constrains the typical length-scale of turbulence. Thick shrouds of ash obscure the flow regime within the column, which as we discuss below may be of a jet-like nature (Kieffer, 1984). From the base of the column a pyroclastic flow moves down slope, and an ash cloud rises above it.

Caldera evolution sequence

Silicic calderas are generally thought to form in volcanoes that have demonstrated highly explosive or very large mass-flux eruptions. Their long histories of development involve extrusive volumes of the order of several hundreds or thousands of cubic kilometers. Eruptive behaviors range from passive lava extrusions to short-lived explosive blasts and the prolonged jetting of large volumes of tephra and gases. Gradual chemical differentiation of underlying, crustal magma chambers may produce a volatile-rich layer at the chamber roof (Hildreth, 1979). During the catastrophic release of overpressured volatiles from the upper portion of such chambers, Smith (1979) has estimated a 10 vol.% drawdown of the magma reservoir. Such a volume may amount to several hundreds of cubic kilometers. Wohletz *et al.* (1984) have simulated such an eruption and have shown that the propagation of a rarefaction wave from the vent down into the chamber (pressurized to 100 MPa) stimulates the vesiculation and fragmentation of the magma such that it erupts as an overpressured jet of hot pumice, ash and gases. Initially the flow from the vent is unsteady, producing propagating shock waves in the atmospheric flow field. Gradually the flow becomes steady with the generation of a high standing eruption column that may collapse in a fountain-like manner. After the magma chamber becomes largely depressurized, the buoyant rise of viscous magma through the vent system may produce lava domes and flows.

Plinian eruption columns and their collapse

Descriptions of the AD 79 explosive eruptions of Vesuvius, published by Pliny the Younger, have lead to the specific definition of Plinian phenomena by Walker (1981), which includes high standing (10–50 km) eruption columns that sustain volume fluxes in excess of $10^6\ m^3\ s^{-1}$. These eruption columns are multiphase mixtures of pumice, ash and gases (mostly steam) that show jet-like features at their bases and the rise of

Figure 1. 22 July 1980 eruptive column of Mount St Helens, showing several features common to many explosive eruption phenomena: a vertically rising column of ash and gases with a mushroom-shaped top (the working surface), a laterally moving pyroclastic flow emanating from the base of the column, turbulent eddies of ash, and obscurity of the flow regime within the column. The vertical scale is about 15 km. Photograph by James Vallance

buoyant plumes near their tops (Sparks, Wilson and Hulme, 1978; Wilson, Sparks and Walker, 1980). The flow is generally steady and displays considerable turbulence, which is thought to encourage the mixing of the cooler atmosphere into the column. Heating of admixed atmosphere by hot tephra can be sufficient to cause the column to rise buoyantly. If the atmospheric mixing is insufficient, such that the column remains denser than the atmosphere, the column may collapse, spilling erupted debris and gases to the ground around the vent to produce ground-hugging flows called 'pyroclastic flows'.

Vulcanian and blast-type eruptions

Named after the classical eruptive behavior of Vulcano in the Tyrrhenian Sea near Italy (Mercali and Silvestri, 1891), Vulcanian eruptions are generally described as repeated, cannon-like or staccato bursts of tephra with relatively small volume fluxes ($\ll 10^6\ m^3 s^{-1}$). They form both hemispherically expanding clouds of tephra and gases and buoyantly rising plumes of up to several kilometers height. The highly unsteady flow regime of these eruptions can be accompanied by propagation of atmospheric shocks, temporary development of supersonic, overpressured jets, and the development of laterally moving density currents of erupted ash called 'pyroclastic surges'. The unsteady and overpressured nature of such eruptions have characteristics similar to the phenomena initiating larger Plinian events.

Strombolian and fountaining eruptions

Stromboli, the 'light-house of the Mediterranean' is a volcano that ejects short to prolonged bursts of tephra in ballistic trajectories from the vent. The expelled tephra, in contrast to those produced by the eruptions described above, generally are not supported by an envelope of erupted gases. The rapid expansion of centimeter- to meter-sized gas bubbles propels these tephra through the atmosphere. Where such activity is prolonged, a ballistic fountain is often observed. Because such behavior results in the rapid segregation of tephra from expanding gases, the expansion is nearly adiabatic in contrast to the Plinian and Vulcanian types in which gases remain in contact with the hot tephra and can expand nearly isothermally.

Modeling Approach

The mathematical formulation that we have used has been applied to a wide variety of dispersed, multiphase flows, and it is discussed at length in the book by Ishii (1975). At the heart of the formulation is the assumption that the different materials involved in the flow-field can be treated as individual continua. These continua are superimposed in space and are coupled by the interphase transfer of mass, momentum and energy. Because the different material components are treated as individual continua, the full set of conservation equations must be solved for each material (or 'field'). The interphase transfer of transport quantities (mass, momentum and energy) also requires that all equations for all fields must be solved simultaneously. It is clear that the comprehensiveness of a model forces an approach to the limits of modern computational speed and memory. For example, to model a two-dimensional, time-dependent, high-speed flow of gas and particles of three sizes would require the solution of 16 non-linear partial differential equations (a set of four equations for the gas and for each particle size) and 20 additional algebraic equations (equations of state and interphase coupling) with 36 dependent variables. This example does not include mass transfer terms and would be capable only of including turbulent effects in the form of an eddy viscosity; solving more realistic turbulence transport equations, such as those presented by Besnard and Harlow (1988), would at a minimum double the number of dependent variables.

One might thus ask: why undertake numerical modeling if the models are simplified compared with natural phenomena? The example described above shows how complex a numerical solution can be with only three particle sizes, one gas phase and no mass transfer. We know, for example, that volcanoes contain tephra particles ranging in size over several orders of magnitude with variable densities and shapes. There is, moreover, more than one gas species involved in such flows. Mass transfer, in addition, involves the exsolution of volatiles from tephra and their subsequent phase change. Although we can only model very crude approximations of such complex natural processes, the approximations obtained provide a behavioral insight that simply could not be obtained by intuition alone. The reason for this

'beyond intuition' probe of natural processes derives from the intrinsic non-linearity of the governing equations; many non-linear processes are too complicated for mental solution even at an intuitive level; hence, the necessity of a sophisticated computing approach. Overall, we believe that gaining an understanding of relatively simple analogs is a necessary prerequisite before grasping the greater complexities of nature. This reasoning is also the justification for laboratory experimentation. Numerical simulation, however, overcomes the problems of dynamic similarity that often plague laboratory analogs.

Mathematical formulation

Our modeling effort has focused on solving the following set of the complete Navier–Stokes equations, which describe a two-phase flow of compressible gas and incompressible solid particles:

$$\frac{\partial(\theta_g\rho_g)}{\partial t} + \nabla\cdot(\theta_g\rho_g\mathbf{u}_g) = J \quad (1)$$

$$\frac{\partial(\theta_s\rho_s)}{\partial t} + \nabla\cdot(\theta_s\rho_s\mathbf{u}_s) = -J \quad (2)$$

$$\frac{\partial(\theta_g\rho_g\mathbf{u}_g)}{\partial t} + \nabla\cdot(\theta_g\rho_g\mathbf{u}_g\mathbf{u}_g) = -\theta_g\nabla p + K_g|\Delta\mathbf{u}| + J\mathbf{u}_g + \theta_g\rho_g\mathbf{g} - \nabla\cdot\tau_g \quad (3)$$

$$\frac{\partial(\theta_s\rho_s\mathbf{u}_s)}{\partial t} + \nabla\cdot(\theta_s\rho_s\mathbf{u}_s\mathbf{u}_s) = -\theta_s\nabla p + K_s|\Delta\mathbf{u}| - J\mathbf{u}_s + \theta_s\rho_s\mathbf{g} - \nabla\cdot\tau_s \quad (4)$$

$$\frac{\partial(\theta_g\rho_g I_g)}{\partial t} + \nabla\cdot(\theta_g\rho_g I_g\mathbf{u}_g) = -p\nabla\cdot[\theta_g\mathbf{u}_g + \theta_s\mathbf{u}_s] + R_g + |K_g|(\Delta u_g)^2 + J_e - \tau_g : \nabla\,\mathbf{u}_g \quad (5)$$

$$\frac{\partial(\theta_s\rho_s I_s)}{\partial t} + \nabla\cdot(\theta_s\rho_s I_s\mathbf{u}_s) = R_s - J_e - \tau_s : \nabla\,\mathbf{u}_s \quad (6)$$

This formulation for two-phase flow (symbols are defined in the notation listing), originally presented by Harlow and Amsden (1975), is very general, and has been successfully applied to a wide variety of flows. These flows range from the bubbly flow past an obstacle to star formation processes (Hunter *et al.*, 1986). An important aspect of equations (1) through (6) is that they are cast in terms of volume-averaged quantities. The elemental volumes over which the differential equations are solved are necessarily much larger than the size of individual solid particles carried by the flow. This restriction is required for the continuum approach to be valid (Travis, Harlow and Amsden, 1975).

Equations (1) and (2) describe the conservation of mass for the gas and the solid phases, respectively. The left-hand side of these equations represents the sum of the temporal and spatial changes of mass that are contained within a representative elemental volume. The right-hand sides represent the contribution to the gas phase by mass diffusion out of the solid phase.

Momentum conservation for the gas and solid phases is respectively expressed by equations (3) and (4). They state that the transient momentum changes within and through a volume element are just balanced by the sum of the forces due to the combined pressure gradient, the interphase momentum transfer (drag), the gravitational acceleration, the momentum exchanged by interphase mass transfer, and the viscous and turbulent stresses. Because explosive volcanic eruption columns have high Reynolds numbers, turbulent forces greatly dominate over viscous ones, such that the last balancing term can then be represented by the divergence of the strain-rate tensor using an eddy viscosity. The two-dimensional stress tensor has the following form in cylindrical coordinates, which crudely represents the Reynolds stress tensor:

$$\tau = -\theta\rho\nu_e\begin{bmatrix} 2\dfrac{\partial u}{\partial r} & 0 & \left[\dfrac{\partial v}{\partial r}+\dfrac{\partial u}{\partial z}\right] \\ 0 & 2\dfrac{u}{r} & 0 \\ \left[\dfrac{\partial v}{\partial r}+\dfrac{\partial u}{\partial z}\right] & 0 & 2\dfrac{\partial v}{\partial z} \end{bmatrix} \quad (7)$$

The eddy viscosity, ν_e, is constrained by observed eddy length-scales and numerical considerations, and it plays an important role in determining the mixing of the atmosphere into the eruption column (Valentine and Wohletz, 1989a). Although this description of turbulence is very crude and a more detailed calculation is being sought (e.g., Besnard and Harlow, 1988), we note that empirically derived turbulence representations have a direct relationship with measurable physical

features of flows, and that the theoretically derived ones are only poorly coupled with observation. For two-dimensional solutions, the momentum equations must be written for both the axial and radial components of velocity of the gas and solid phases.

The conservation of specific internal energy within a volume element for the gas and solid phases are given by equations (5) and (6), respectively. The temporal and advected energy changes are equated to the sum of pressure-volume work, interphase heat transfer, heat exchanged by phase changes, and energy dissipation by viscous stresses and turbulence. The gas phase also experiences changes in internal energy caused by interphase drag-induced dissipation.

When written in expanded form, these equations comprise a system of eight, non-linear, partial differential equations. Closure of the equations is obtained by applying algebraic relations that describe the equations of state for the materials, the relationship between volume fractions, and interphase coupling (see Valentine and Wohletz (1989a) for a detailed presentation of these terms). These algebraic closure equations thus account for the volume-averaged effects of processes that happen on a smaller scale than the elemental volume used for differentiation; for example, the drag of fluid on individual particles. The very nature of this mathematical formulation requires that the microphysics are treated in only an averaged sense. Thus many small-scale physical processes that are undoubtedly of importance in some volcanic phenomena are not included. Examples of such microphysics include particle–particle collisions, the particle-wake interactions, and distributions of gas bubble sizes in decompressing magmas. In principle the volume-averaged effects of any such process can be included in the governing equations. For example, in detailed simulation of a dense pyroclastic flow, one can introduce a pressure term in the equations for the particle phase, accounting for the normal stress produced by shearing grain flows. To date our simulations have focused on the large-scale processes where most of the microphysical behavior is thought to make negligible contributions.

A comment is in order, relating the role of turbulence in the governing equations and how atmospheric entrainment is calculated. Previous eruption column models have been limited to one-dimensional, single-phase fluid approximations (see Woods (1988) for a recent review and improvement of previous model attempts). In these approximations, a source term is required on the right-hand side of the conservation of mass equation in order to account for the relatively cool atmosphere added to the flow by entrainment (i.e., the entrained fluid is added to the one-dimensional system). In our calculations, the atmosphere is part of the computational domain, and its entrainment naturally occurs as a result of turbulent diffusion in the momentum equation. In other words, the turbulent stress term in equations (3) and (4) produces a 'force' that causes fluid movement in the same manner as any of the other terms in the momentum balance. As a result where a velocity gradient is present, adjacent parts of the flow-field will diffuse or interpenetrate into each other; the amount of interpenetration is proportional to the velocity gradient. Thus the gross effects of entrainment are included in the calculations. The details of this entrainment, which involve a Kelvin–Helmholtz instability, are not strictly calculated but are thus solved in an averaged sense.

Although equations (1) through (6) are fairly comprehensive in that they include no restricting assumptions that might affect dynamic similarity, caution is required in applying their solutions to nature in the sense that they do not calculate 'real' volcanoes. Because of the turbulence simplification and microphysical assumptions discussed above, the calculations are only valid in showing general eruption behaviors and relative variations that result from changes in initial and boundary conditions. We do not believe that it is realistic to apply numbers calculated by our models directly to natural systems, although that is a goal that von Neumann believed is obtainable. Nevertheless, we can learn about the relative sensitivity of physical parameters involved, which is valuable for the interpretation of field observations.

Computer adaptations

Although mathematical solution techniques are available for attempting to obtain analytical solutions to the above equation set, it may be exceedingly difficult or impossible to obtain meaningful results after the required simplifications are made. Hence we have applied a numerical solution technique by finite differences (Ferziger, 1981). We

begin by expanding the equations above into partial derivative form, using cylindrical coordinates (r, z, θ) with azimuthal symmetry about the z axis, centered at the vent. The difference scheme used to discretize the partial derivatives on a spatially constant and temporally incremented grid was chosen to balance the accuracy and stability with considerations of economy and versatility (Harlow and Amsden, 1975). Although the solution scheme described below is mainly of an Eulerian type of fixed cell locations, Lagrangian marker particles following the flow allow resolution of the intermixing of flow-fields.

Finite difference solution scheme

A mixed, implicit–explicit solution method, developed by Harlow and Amsden (1975), was chosen because of its economy and because inherent numerical instabilities are easily rectified. A purely implicit differencing method of temporal derivatives is generally more stable but can be computationally slower. For example, the first term on the left-hand side of the continuity equation is written:

$$\frac{\partial \rho}{\partial t} \simeq \frac{\rho^{n+1} - \rho^{n}}{\delta t} \qquad (8)$$

where the approximation signifies that of the finite differencing, and the index n represents the time-step, such that there are $n = t/\delta t$ time-steps of duration δt in a time period t. This forward differencing scheme explicitly gives the new value of ρ, ρu, ρv, or ρI with a truncation error of the order of δt. Velocities are placed at cell edges for differencing advective terms to best model fluxes through the cell edges. In order to circumvent stability problems in using cell-edge values of vectors, a staggered grid is defined for which i and j are the cell center indices, and the advective term in the continuity equation is:

$$\frac{\partial(\rho v)}{\partial z} \simeq \frac{1}{\delta z}\left[\rho_{i,j} v_{i,j+1/2} - \rho_{i,j-1} v_{i,j-1/2}\right] \qquad (9)$$

which holds for flow in the positive z direction. Such a scheme is called 'donor cell' or 'upwind' differencing, which ensures that the value advected into the specific cell originates 'upstream'. This scheme suppresses numerical instability, but steep gradients tend to be smeared over several cells, and the truncation error is kept to first order. For this reason, shocks in supersonic flows are not uniquely defined, but their effects can be distinguished easily in the solutions. Other non-trivial finite differences are those for stress tensors, which are solved for cell-edge values in the momentum equation and cell center quantities in the energy equation (Horn, 1986). For momentum and heat exchange terms in the conservation equations, an implicit form was chosen, because it is simple and unconditionally stable. In general the calculational time-step proceeds by obtaining advanced time values for all scalar variables in the mesh, followed by a second iteration, during which new velocities are calculated, using new densities.

Because the systematics for solving the equation sets described above have been developed previously at Los Alamos for generalized application to hydrodynamics (e.g. Harlow and Amsden, 1975), it has been convenient to borrow sections of FORTRAN programs from other codes, making adaptations necessary for the simulation of geological processes. In all cases, stability has been verified for the difference techniques (Hirt, 1968), such that we have a high confidence in their application over a large range of flow velocities. In most of our applications we have chosen a spatial resolution of 100 m and a time step of 0.02 s. This choice easily satisfies the Courant condition while allowing us to simulate the two-dimensional flow-fields of several tens of square kilometers. We note, however, that for the high-speed flow regime that may initially exist in the vent, our codes can automatically adjust the temporal and spatial step of differencing in order to resolve steep pressure gradients and shock waves.

Numerical output, graphical representation, and analytical approach

In general, numerical results of each time-step are dumped to disk storage for retrieval in the next time-step, restarting the calculation, and generating tabular and graphical results. A typical calculation of 200 s of eruption time produces over 20 000 pages of tabulated numbers. A post-processor code can be applied to the dump files for various graphical outputs, including vector and contour plots and movies thereof. We have found that analysis of such voluminous results is time consuming and difficult, such that a detailed study of an eruption simulation with initial and boundary conditions set to model a given volcano

is analogous to a geological field study in which numerous field locations are examined to describe eruption effects and deposits.

It is instructive and useful to study the simulation results for consistency with laboratory analogs and predictions, based upon other analytical solutions. As discussed below, aspects of the physics of high-speed flows are known from laboratory experiments, and thus our computer results can be tested for their ability to reproduce known experiments. Once credibility has been established for a computer code, its results are considered to be 'data' in that they are simply mathematical representations of physical parameters, as are, for example, X-ray analyses of rock chemical compositions, for which X-ray intensities are converted by mathematical tools into numbers of chemical significance.

Unsteady Discharge (Blast-type) Eruptions

The concept of blast-type eruptions was recently given a descriptive review by Kieffer (1982,1984), and it includes eruptions that show highly unsteady, supersonic flow with notable propagations of shock waves, either as bow shocks that precede expulsions of tephra or as standing (Mach disk) shocks, that develop within supersonic jets of tephra and gases. Such eruptions are short-lived and in many places produce pyroclastic surge deposits of tephra. By analogy to large chemical or thermonuclear explosions, the presence of base surge deposits are often an earmark of highly unsteady flow and shock propagation (Glasstone and Dolan, 1977). As discussed above such eruptive phenomena are associated with the initial phases of Plinian eruption and Vulcanian bursts.

Analysis of blast conditions

Wohletz *et al.* (1984) modeled large eruptive blasts associated with Plinian eruptions that occur during caldera-forming events. Assuming that an overpressured magma chamber can be opened nearly instantaneously to the atmosphere by large-scale vent-rock failure, analogy to shock-tube physics (Wright, 1967) is a convenient way to predict flow phenomena and to test the ability of our computer code to provide solutions that

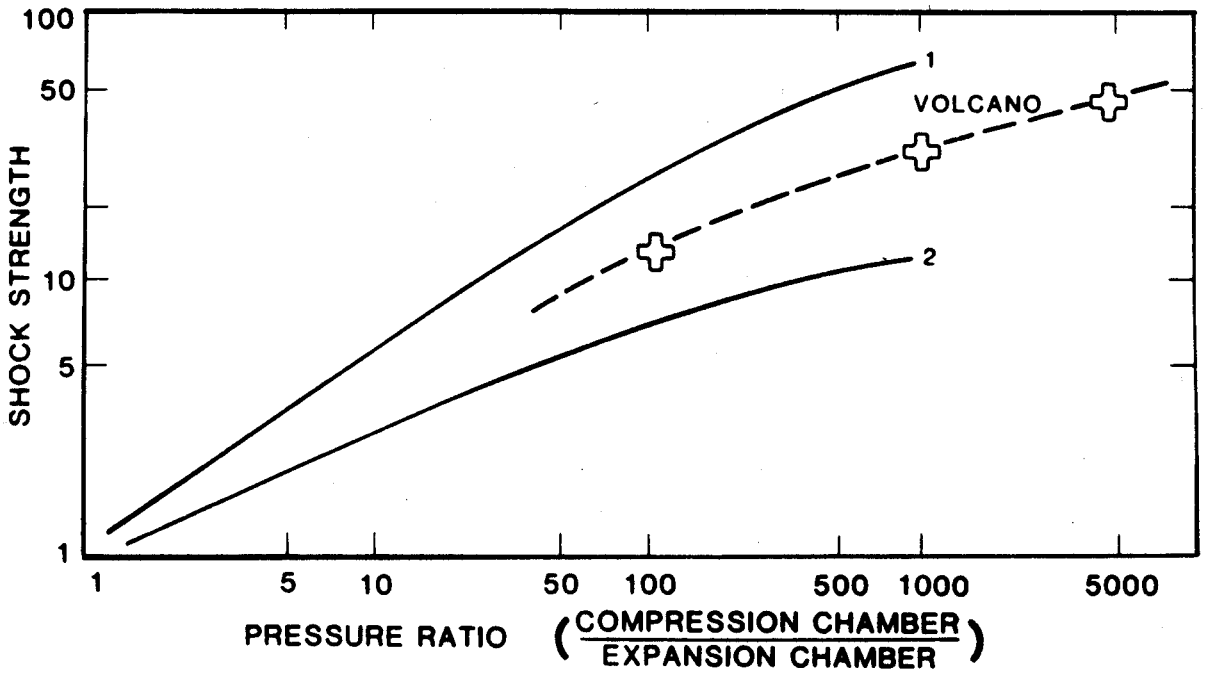

Figure 2. Plot of shock strength versus chamber overpressure for two shock-tube cases (Wright, 1967) and a volcano model. Curve 1 shows results for compressed hydrogen expanding into air compared with those of compressed air expanding into air (Curve 2). The crosses plot expansion of a hypothetical volcanic steam and ash mixture

emulate those physics. These flows are described from consideration of mass and momentum conservation respectively written for one-dimensional, inviscid flow:

$$\frac{\partial \rho}{\partial t} + \rho \frac{\partial u}{\partial x} + u \frac{\partial \rho}{\partial x} = 0 \tag{10}$$

$$\frac{\partial u}{\partial t} + u \frac{\partial u}{\partial x} + \frac{1}{\rho} \frac{\partial p}{\partial x} = 0 \tag{11}$$

Letting $f = \int c d\rho/\rho$, integrating from ρ_0 to ρ where $c = [\gamma(\partial p/\partial \rho)]^{1/2}$, and substituting characteristic velocities, $dx/dt = u \pm c$, the conservation equations can be rewritten algebraically as:

$$\frac{\partial}{\partial t}(f+u) + (u+c)\frac{\partial}{\partial x}(f+u) = 0 \tag{12}$$

$$\frac{\partial}{\partial t}(f-u) + (u-c)\frac{\partial}{\partial x}(f-u) = 0 \tag{13}$$

Using ideal equation of state where $p\rho^{-\gamma}$ equals a constant, the solution for f is, using the Riemann invariant for free expansion (Courant and Friedrichs, 1948):

$$f = \frac{2c_0}{\gamma - 1}\left[\left(\frac{p}{p_0}\right)^{(\gamma-1)/2\gamma} - 1\right] \tag{14}$$

Now, with Rankine–Hugoniot expressions for mass, momentum and energy conservation across a shock wave (e.g., Shapiro, 1953), the flow-field of a shock tube can be described fully by the following algebraic expressions:

$$\frac{U_s}{c_0} = M = \left(\frac{y+\mu}{1+\mu}\right)^{1/2} \tag{15}$$

$$\frac{u}{c_0} = \frac{(1-\mu)(y-1)}{[(1+\mu)(y+\mu)]^{1/2}} \tag{16}$$

$$\frac{\rho}{\rho_0} = \frac{\mu + y}{1 + \mu y} \tag{17}$$

$$\frac{T}{T_0} = \frac{y(1+\mu y)}{\mu + y} \tag{18}$$

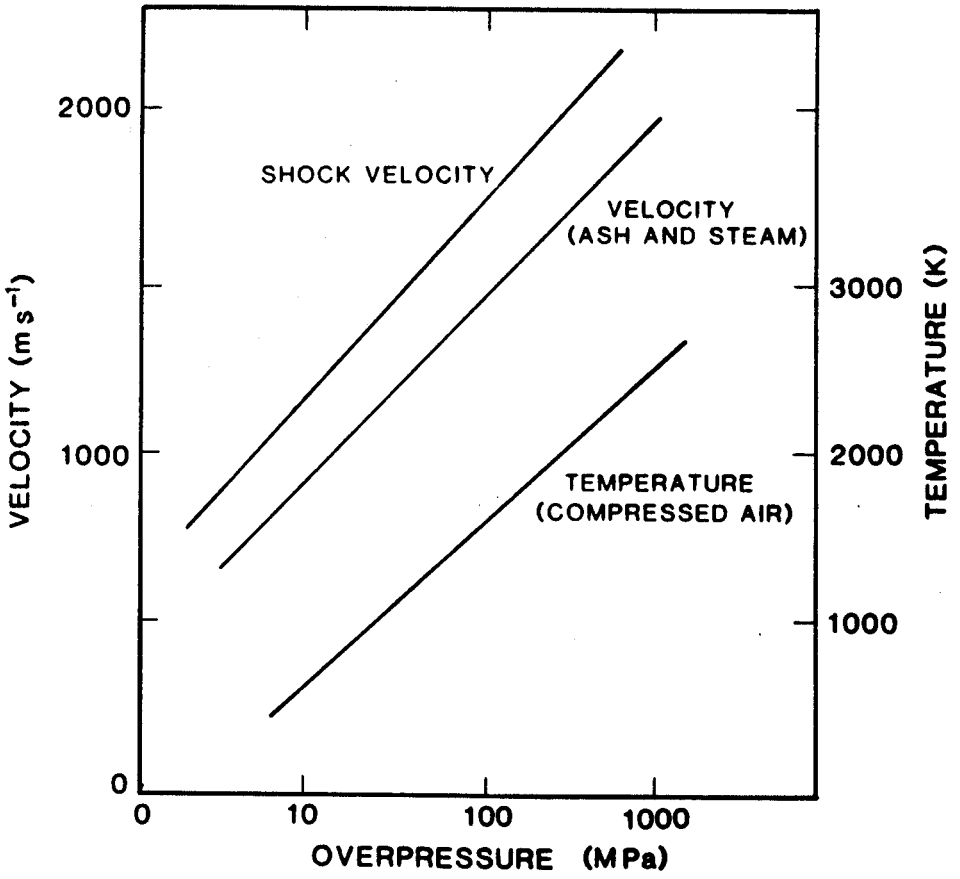

Figure 3. Plot of shock (ash and steam) and compressed air velocities and temperatures of the Bandelier Tuff eruption from the analytical solutions (equations (15) through (18)) of the shock-tube physics

for which U_s is the shock speed, c_0 is atmospheric sound speed, the Mach number is $M = U_s/c_0$, the limit of isentropic expansion is $\mu = (\gamma - 1)/(\gamma + 1)$, and the shock strength is $y = p_2/p_0$, which is a transcendental function of the atmospheric pressure, p_0, and chamber pressure, p_1 (Wohletz *et al.*, 1984). The predictions of y and subsequent flow-field variables are described in Wohletz *et al.* (1984) and are summarized in Figures 2 and 3.

Blast calculation results

We have found that our numerical codes model shock-tube physics for two dimensions well (Figure 4). An application of the KACHINA code (Wohletz *et al.*, 1984) simulated a blast-type eruption from a magma chamber at $p_0 = 100$ MPa, $T_0 = 1273$ K, and being 8.7 wt.% oversaturated with water. The resulting jet-like flow (from a vent with a hydraulic radius of about 100 m) showed a bow shock of 3 MPa overpressure, propagating away from the vent at about 700 m s^{-1}, followed by an expanding steam and ash column. Unsteady flow within the column continued for several minutes as a rarefaction wave propagated down the conduit, decompressing and accelerating the steam and ash from 300 to 500 m s^{-1}. Because the rarefaction wave

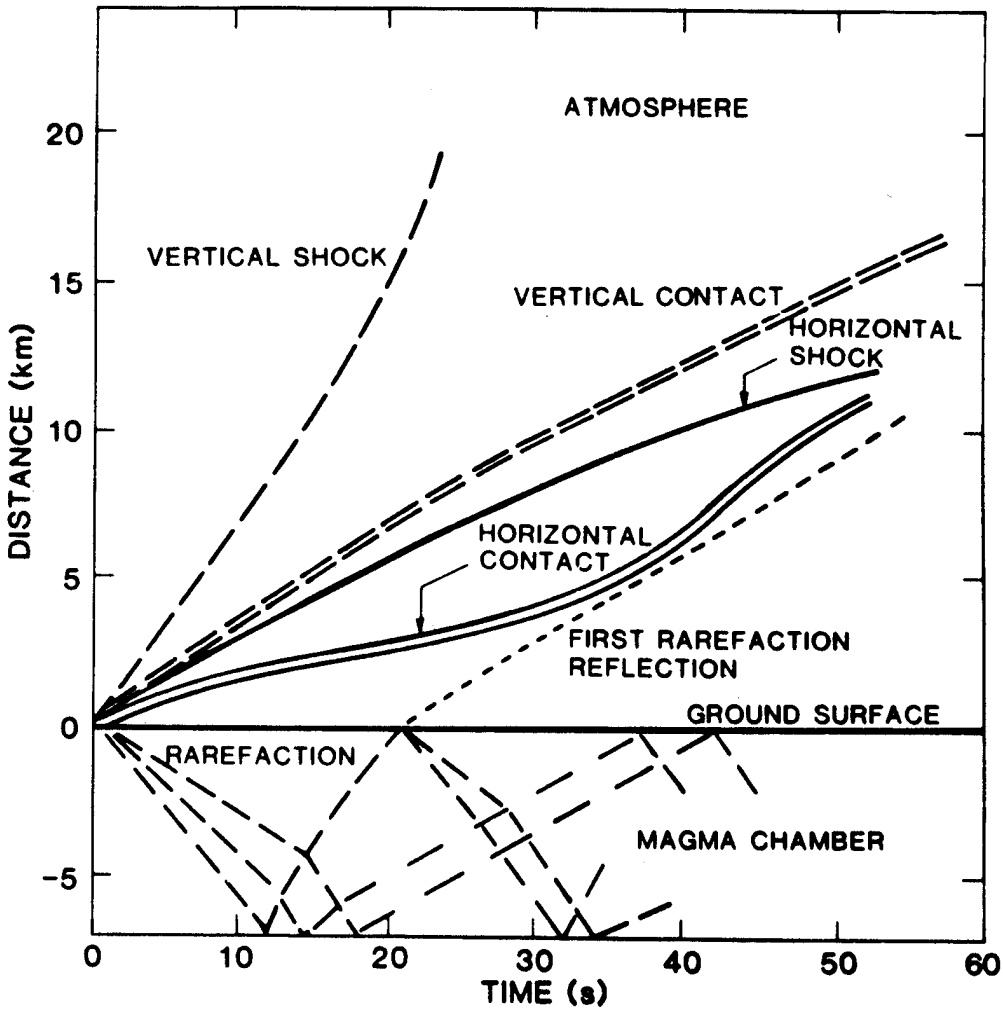

Figure 4. Distance–time plot for the computer simulation of the blast thought to have initiated the eruption of the Bandelier Tuff. The plot is analogous to an ideal one for a shock tube with the propagation of a shock wave into the atmosphere, while a rarefaction wave propagates down and reflects within the conduit and magma chamber. The contact surface marks the front of tephra and steam accelerated up and out of the vent. Both the vertical and horizontal components are shown for these waves

reflected off chamber walls, it caused surging flow out of the vent and development of a fluctuating Mach disk shock that added to the blast phenomena. These results are shown in Figures 5 through 7.

One interesting aspect of these calculations for blast eruptions is the ability of the KACHINA code to calculate the temporally varying flow regime within the conduit, and hence the bulk density, velocities, pressures, and temperatures at the vent plane. Figures 5 and 6 show a downward propagating rarefaction wave within the conduit, above which marker particles have accelerated upward through the vent. The rarefaction wave decompressed the magma to about 18 MPa at the vent (Figure 6), during which the magma expanded from a supercritical water and solids mixture into a mixture of 'fragmented' steam and ash before exiting through the vent. The spacing of the marker particles is proportional to the magma bulk density, such that below the rarefaction, the magma moved slowly as a viscous liquid. The cells surrounding the conduit simulated incompressible country rock, which could deform as highly viscous Newtonian fluid (an end-member state of the solid phase) where shear and normal stresses were high. This feature of the KACHINA model allowed a crude simulation of vent widening by erosion (Figure 5).

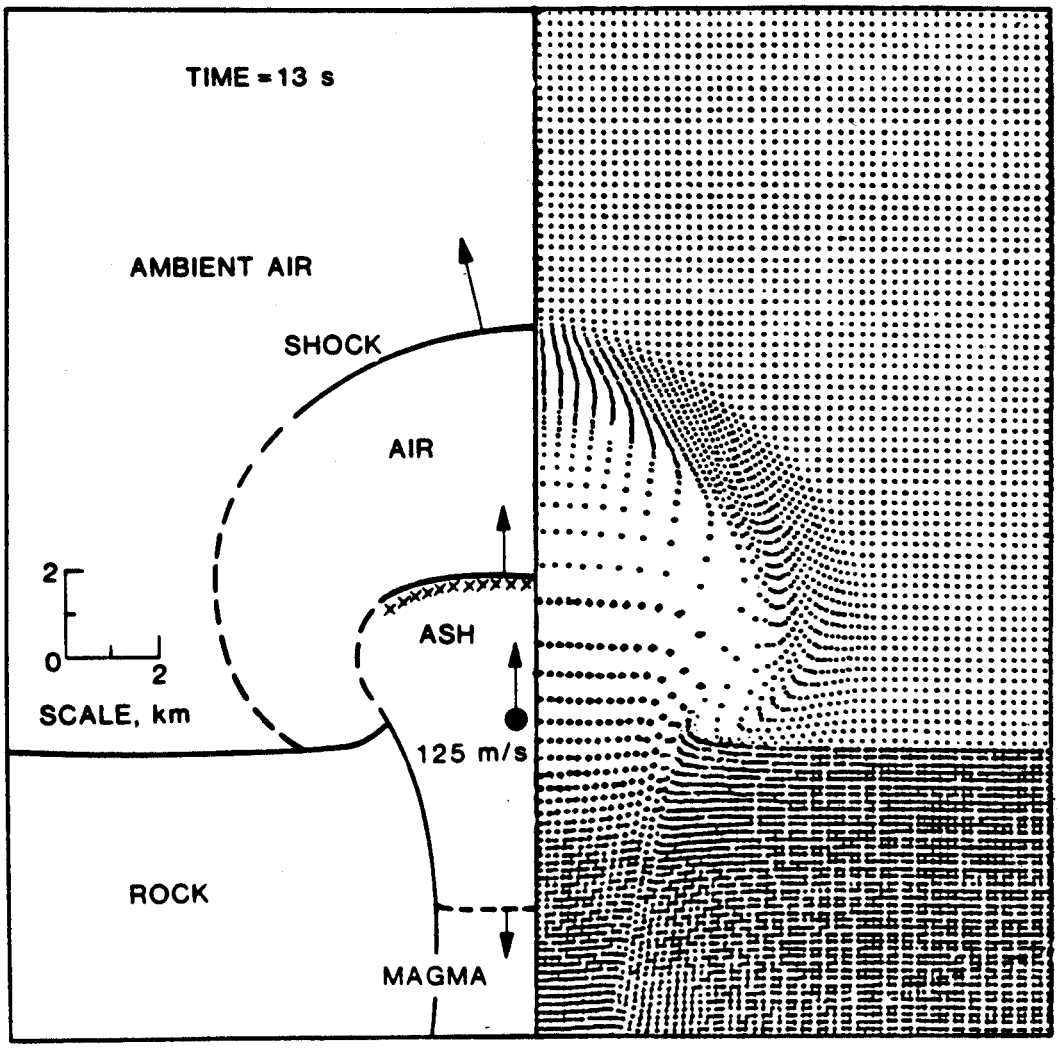

Figure 5. Schematic representation and marker particle plots at 13 s of simulated blast eruption time, showing the shock wave, ash contact and the rarefaction wave in the vent conduit

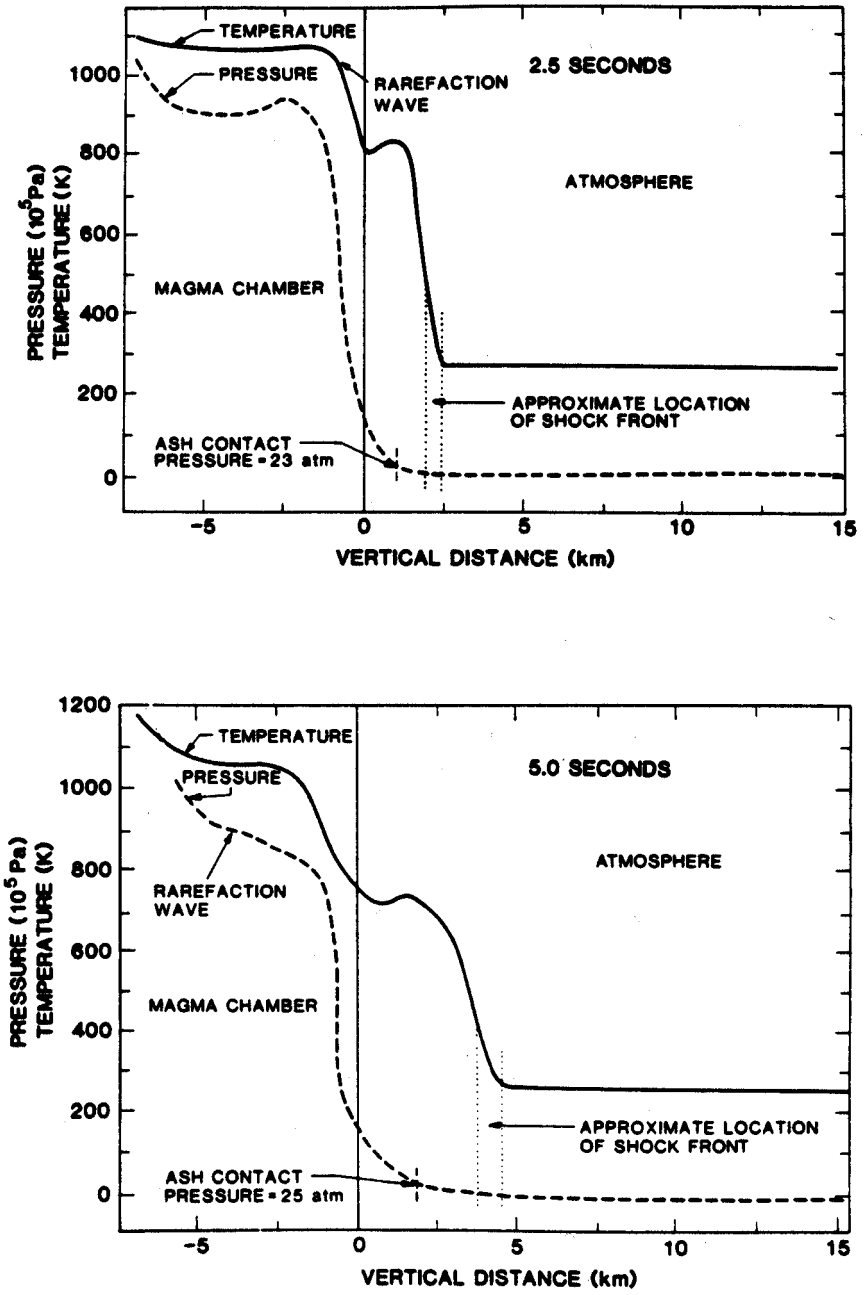

Figure 6. Profiles of pressure and temperature versus distance at 2.5 and 5.0 s after initiation of the simulated eruptive blast. Note the effects of the rarefaction wave upon the magma chamber overpressure, such that the vent plane pressure is about 18 MPa. The location of the ash front (contact) behind the bow shock is calculated by the position of Lagrangian marker particles

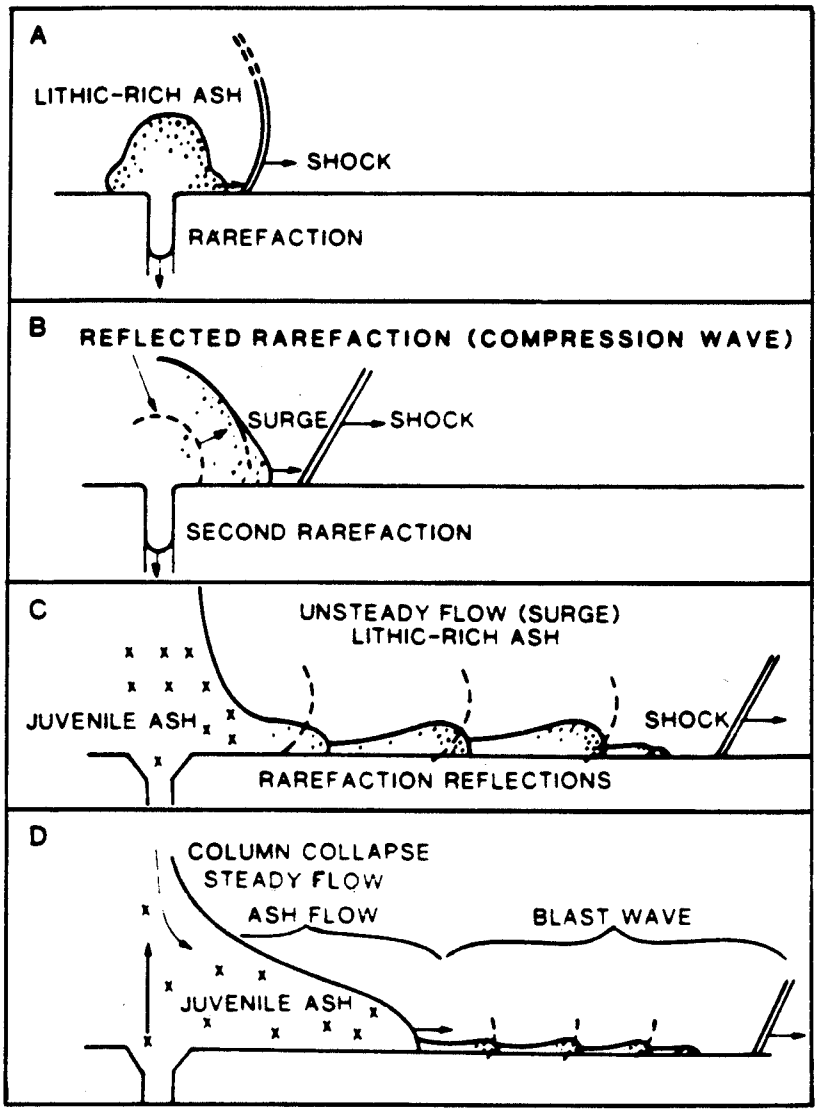

Figure 7. Developmental stages of a blast eruption followed by Plinian column collapse. The blast wave consists of a leading bow shock and trailing surges of tephra in which Mach disk shocks form in response to a wide and nearly hemispherical flaring of the overpressured jet as it expands into the atmosphere

Steady Discharge Eruptions

Many explosive eruptions, especially those classified as Plinian, are thought to involve relatively long periods of approximately steady mass discharge once a vent has been opened (Walker, 1981). Depending on vent flow conditions, eruption columns may either rise as buoyant plumes from which tephra is deposited by fallout, or collapse in a fountaining manner from which tephra is emplaced by laterally flowing density currents (Sparks, Wilson and Hulme, 1978; Wilson, Sparks and Walker, 1980; Valentine and Wohletz, 1989a). Within the framework of our simulations, the conditions that determine whether an eruption column is positively buoyant or forms a negatively buoyant fountain can be shown as a function of three dimensionless numbers (Figure 8). These numbers are:

$$T_{gm} = \frac{p_e - p_{atm}}{(\rho_m - \rho_{atm})gR_v} = \frac{\text{pressure driving force}}{\text{buoyancy force}} \quad (19)$$

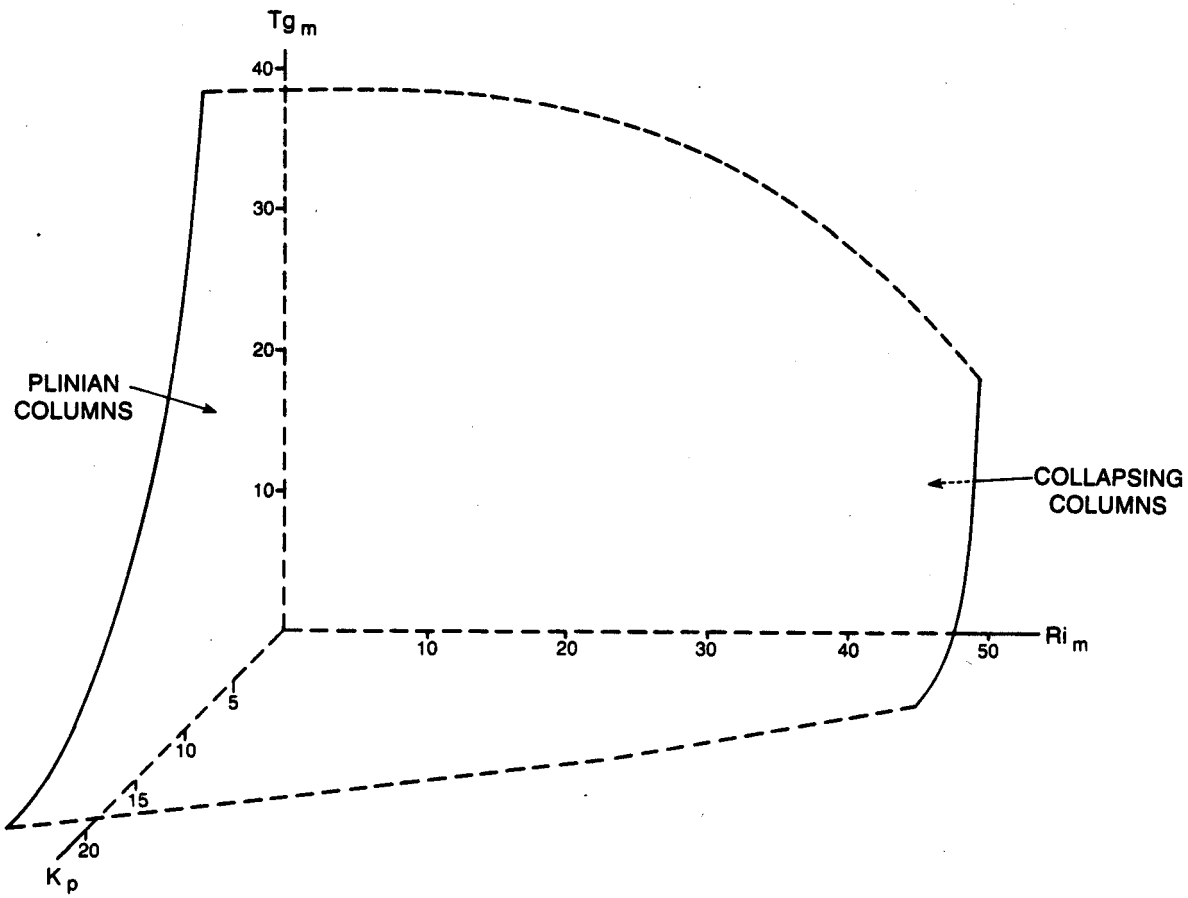

Figure 8. Plot of the collapse criterion for eruption columns in forming fountains. This plot is for a single tephra particle size and shows the control by T_{gm}, Ri_m, and K_p, as defined by the exit conditions. Exit conditions plot above the surface for high standing Plinian columns, whereas those plotting below the surface produce collapsing columns or negatively buoyant fountains that lead to pyroclastic flow phenomena. This criteria holds for eruptions of similar particle size

$$Ri_m = \frac{\rho_m v_e^2}{(\rho_m - \rho_{atm})gR_v} = \frac{\text{inertial force}}{\text{buoyancy force}} \quad (20)$$

$$K_p = \frac{p_e}{p_{atm}} = \frac{\text{exit pressure}}{\text{atmospheric pressure}} \quad (21)$$

for which T_{gm}, the thermogravitational number, is a function of the exit (p_e) and atmospheric (p_{atm}) pressures, erupted column density (ρ_m) and atmospheric density (ρ_{atm}), gravitational acceleration (g), and vent radius (R_v); Ri_m is the Richardson number, including the square of the exit velocity (v_e); and K_p is the pressure ratio. In order to arrive at the collapse criterion in Figure 8, we have considered eruptions with the same initial magma temperature (1200 K) and tephra particle size (0.02 mm). A more comprehensive treatment would also include systematic variations of these parameters. We note that our simulations of steady flow eruptions, applying the DASH code (Valentine and Wohletz, 1989a), were performed with a computational domain of 7 km × 7 km, and it is possible that some columns that rose out of the domain might have collapsed from yet higher elevations. Nevertheless, the dimensionless numbers given above have a strong physical significance in determining the behavior of erupted columns. It is their relative influence that has been demonstrated by the numerical experiments.

Plinian eruption columns

The term 'Plinian column', as discussed above, refers to eruptive phenomena of high standing,

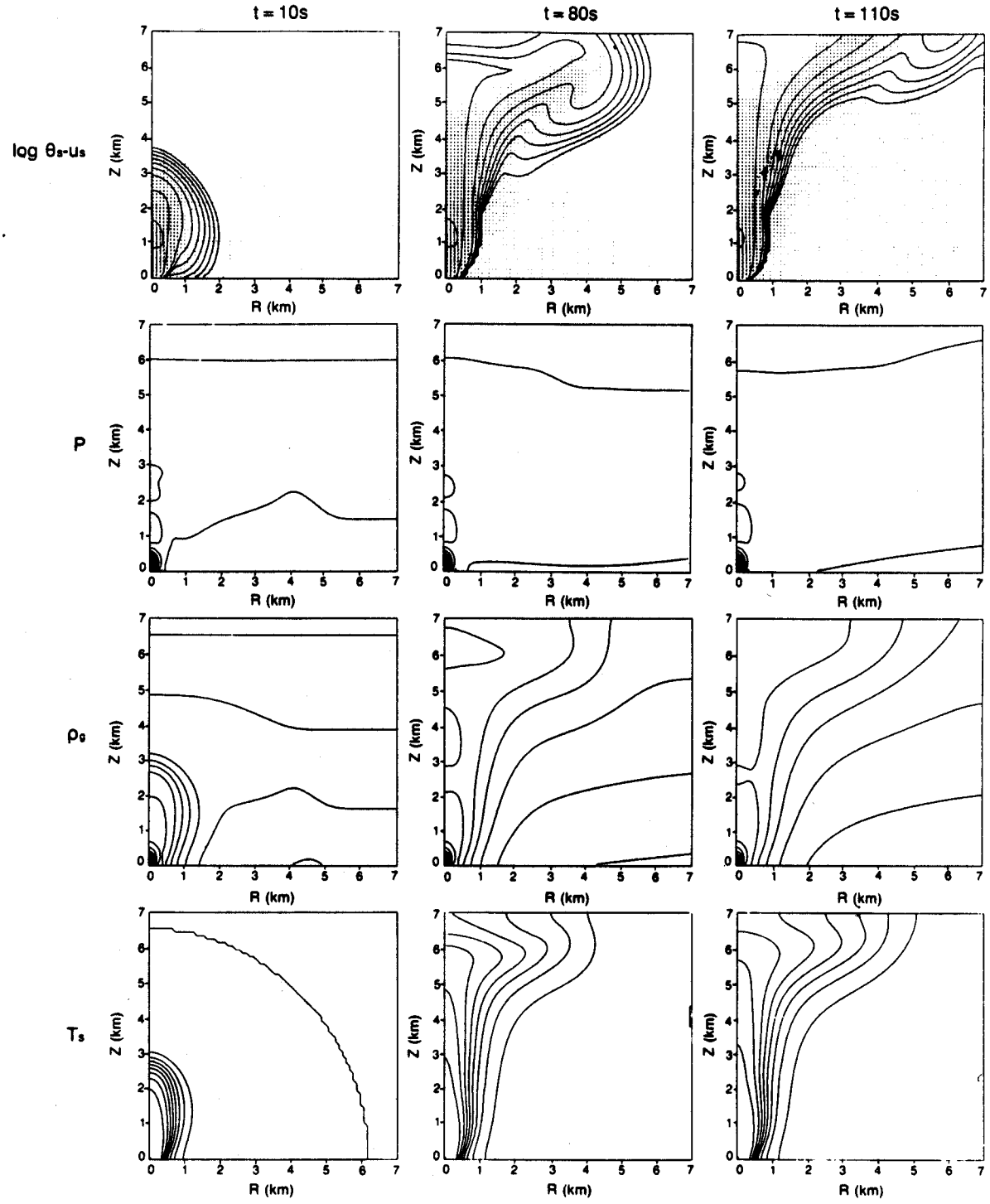

Figure 9. Numerical eruption simulation of a Plinian column. Contour plots of log θ_s with u_s, p, ρ_g, and T_s are shown for three times after the initiation of discharge (10, 80 and 110 s). The innermost log θ_s contour corresponds to a solid volume fraction of 10^{-3}, and each contour outward represents an order of magnitude decrease in that value. Maximum flow speeds of about 400 m s^{-1} are attained in the basal 2 km of the column. The exit pressure of this eruption is 0.69 MPa, and the initial atmospheric pressure signal is shown in the pressure and gas-density plots at $t = 10$ s as a perturbation in the ambient values. T_s contours are drawn at 100 K intervals, starting at 1200 K at the vent, so that the outermost contour corresponds to 400 K. Note that as with all calculations, the atmosphere is initially density stratified and isothermal at 300 K

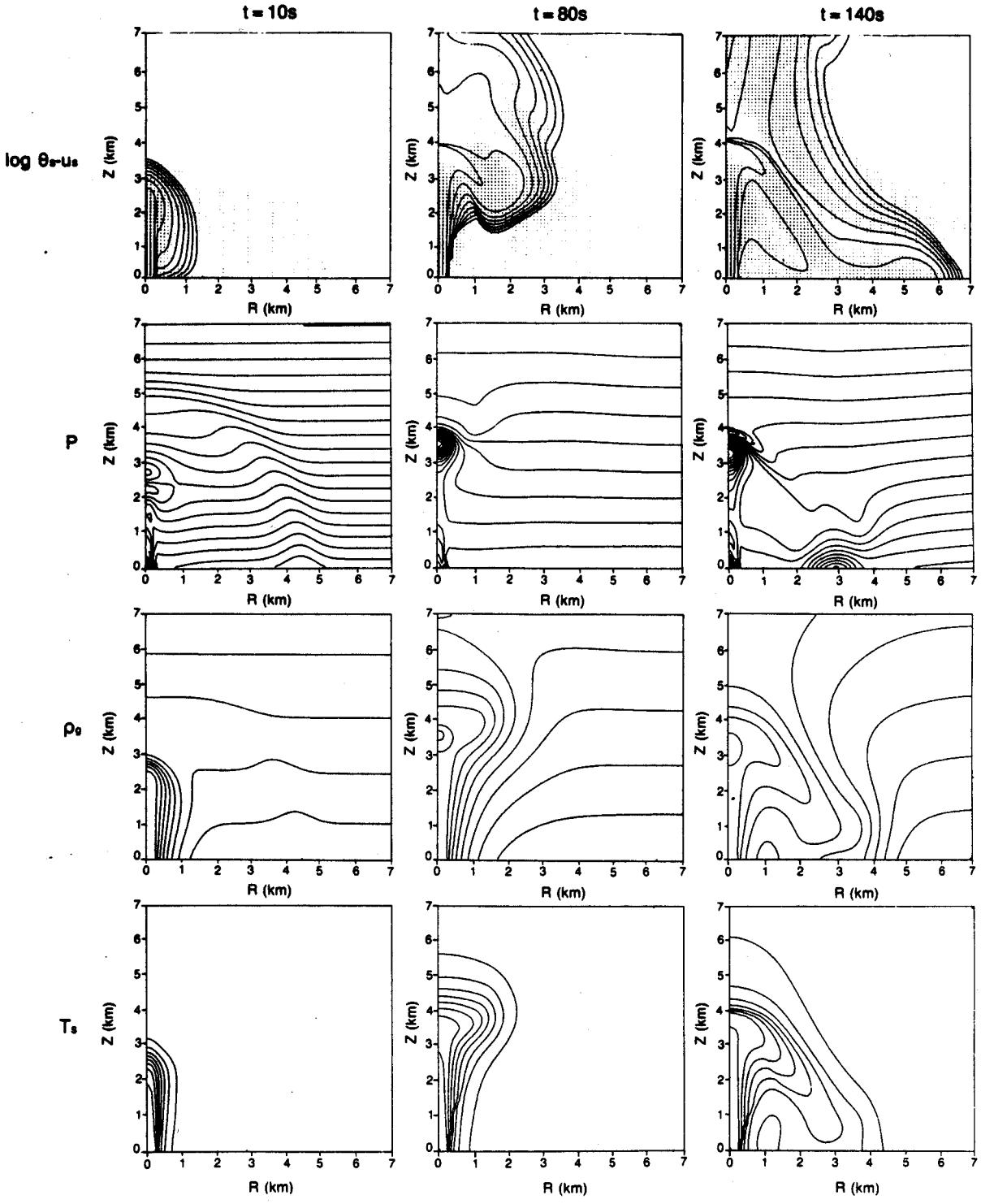

Figure 10. Numerical eruption simulation of collapsing column or negatively buoyant fountain. Contour plots are similar to those in Figure 9 and are shown for simulated eruption times of 10, 80 and 140 s. The exit pressure is atmospheric and maximum speeds are about 300 m s^{-1} at the exit plane. Note that the atmospheric pressure signal at $t = 10$ s is better resolved than that shown in Figure 9, due to the lower pressure of this eruption, allowing the drawing of more closely spaced pressure contours. High-pressure cells are located at the elevation of collapse and where the collapsing flow impinges upon the ground. The contour plot of ρ_g at $t = 140$ s shows how hot, relatively low-density gas is dragged beneath the relatively high-density atmosphere, producing an unstable situation where the hot gas tends to rise out of the basal flow. This situation in turn leads to development of an ash cloud that buoyantly rises above the basal pyroclastic flow

buoyant plumes of gas and tephra. Some results of an example simulation, producing an eruption column that exits the computational domain, are shown in Figure 9. As the flow initially exits the vent, it rapidly flares, owing to expansion from overpressure and the resistance of the atmosphere. The top of the column develops vorticity where it pushes against the atmosphere, and it is termed the 'working surface', analogous to features seen in laboratory simulations of supersonic jets. As time progresses, the working surface rises and, in the last snapshot, it is buoyantly rising out of the computational domain. In the two late-time snapshots, a flaring structure typical of laboratory overpressured, supersonic jets (Kieffer and Sturtevant, 1984) is evident. It is a result of the Prandtl–Meyer expansion of the jet as it exits the vent. Because the governing equations are the full Navier–Stokes equations with no restrictions on compressibility and other flow properties, the range of flow behaviors from subsonic to supersonic occur naturally in the calculations. Shock discontinuities (e.g., Mach disks), as stated above, are numerically diffused over several cells, and their effects are observable from plots of pressure and density contours and velocity vectors.

Eruption fountains and column collapse

When exit conditions of an eruption column plot below the surface shown in Figure 8, the column takes on a fountain-like character (Fig. 10) that leads to formation of pyroclastic flows. In Figure 10 an example simulation is shown where the ash column rises to an altitude of about 3.5–4.0 km and then descends, forming both inward- and outward-moving pyroclastic flows. A low tephra-concentration cloud continuously rises off the pyroclastic flows, and parts of it convectively flow back and up into the rising ash plume above the fountain. Figure 11 shows some of the properties of the pyroclastic flow at three different times during its evolution. The earliest of these times corresponds to the first impact of the descending flow on to the Earth's surface. A parameter that is interesting from a geologic point of view is the dynamic pressure (Figure 11(b)), showing a complicated time evolution. For example, based upon effects of dynamic pressure, we predict that some locations away from the vent may experience a sequence of initial substrate erosion followed by tephra deposition, while other locations experience the opposite sequence. Because the dynamic pressure can be related directly to bottom shear stress and hence erosion/deposition, we infer that even a simple eruption, such as we have numerically simulated, might lead to a very complex stratigraphy of tephra deposits. Eruptions with different exit conditions show widely varying dynamic pressure histories in their pyroclastic flows, indicating that the level of complexity interpreted from stratigraphic observations is essentially unlimited (Valentine and Wohletz, 1989b).

Mount St Helens simulations

Because eruptive fountaining of tephra leads to emplacement of pyroclastic flows, we have compared simulations of the 1980 eruptions of Mount St Helens to observed features. Kieffer (1981) showed how the 18 May 1980 eruption initially produced an unsteady lateral blast by catastrophic decompression of magma with a reservoir pressure and temperature of 12.5 MPa and 600 K, respectively, a solid-to-vapor mass ratio of 25, and 10–20 s of flow from the vent at about 100 $m\,s^{-1}$. Using these estimated blast conditions, our simulations generally support Kieffer's (1981) jet model. Figure 12 depicts the computed flow-field at 2, 10, 20 and 30 s by overlays of velocity vectors and dust concentration. A supersonic jet structure is evident with a Mach disk shock located about 3.5 km away from the vent at 20 s. In the region just down stream from the shock, the flow speed was about 200 $m\,s^{-1}$, the overpressure was 0.0158 MPa, the solid volume fraction was 0.0047, and the temperature was 550 K. Our numbers vary from those of Kieffer (1981), because our vent configuration (0.2 km wide by 0.3 km high) differs from the 1.0-km-wide and 0.25-km-high vent assumed by Kieffer (1981), and our model included gravity effects. Because of the changes required by our model to accommodate a laterally directed vent, we emphasize that these results are only preliminary.

Later steady eruption conditions that produced pyroclastic flows were modeled using flow parameters of Carey and Sigurdsson (1985) for the Plinian phase of the 18 May 1980 eruption. The results of these calculations are discussed by Valentine and Wohletz (1989b). Most notably, calculated pyroclastic flows moved at speeds over 50 $m\,s^{-1}$ with solid volume fraction increasing at the flow head from about 10^{-4} near the vent to

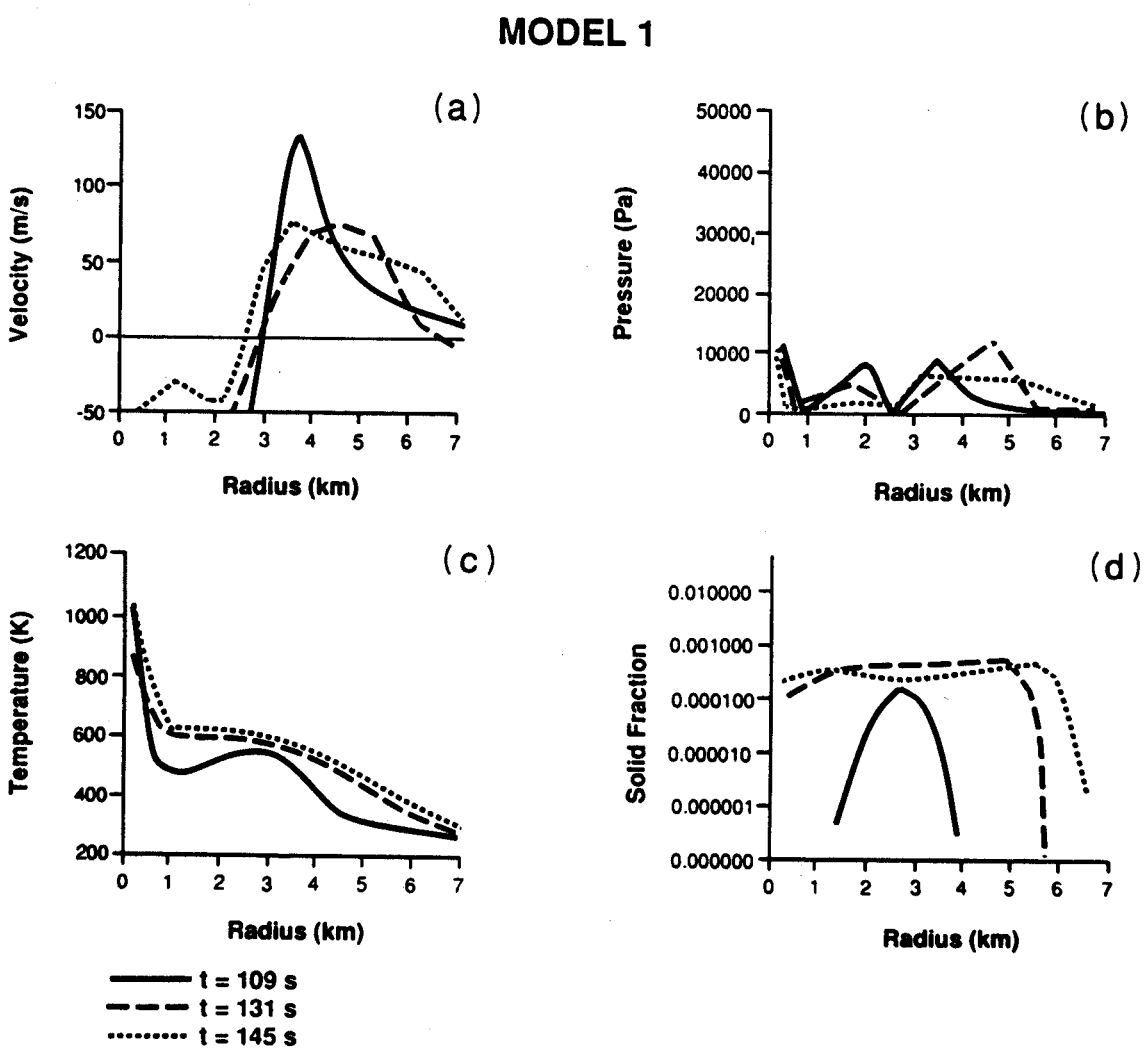

Figure 11. Simulated properties of a pyroclastic flow as functions of distance from the vent center: (a) horizontal velocity; (b) horizontal component of dynamic pressure; (c) temperature; and (d) particle volume fraction. Each of these parameters is shown for three times after the initiation of discharge (t = 109, 131 and 145 s), the earliest of which coincides with the initiation of the pyroclastic flow. For this eruption the flow conditions at the vent (200 m radius) are: velocity of 300 $m\,s^{-1}$, 0.2 mm particle diameter, 0.1 MPa (atmospheric) gas pressure, and a mass discharge of 9.0×10^{-8} $kg\,s^{-1}$

10^{-3} after several kilometers of flow. The damage potential of these flows, measured by their dynamic pressure, reached 1.4 kPa (roughly equivalent to a moderate hurricane) at distances between 1 and 2 km from the vent.

Conduit Flow Calculations

The above simulations have used a wide variety of vent exit conditions. In reality, the exit velocities are strongly coupled to the gas mass fraction, the temperature and pressure, as well as the vent radius. All of these factors have been taken into consideration by Wilson, Sparks and Walker (1980) in a one-dimensional solution of flow within volcanic conduits. Because our solution technique is so very different to the analytical approach used by Wilson, Sparks and Walker (1980) (e.g., we consider two-dimensional solutions, including non-linear and time-dependent processes), we feel that the actual range of exit parameters is still poorly constrained.

We have begun calculations of flow through the

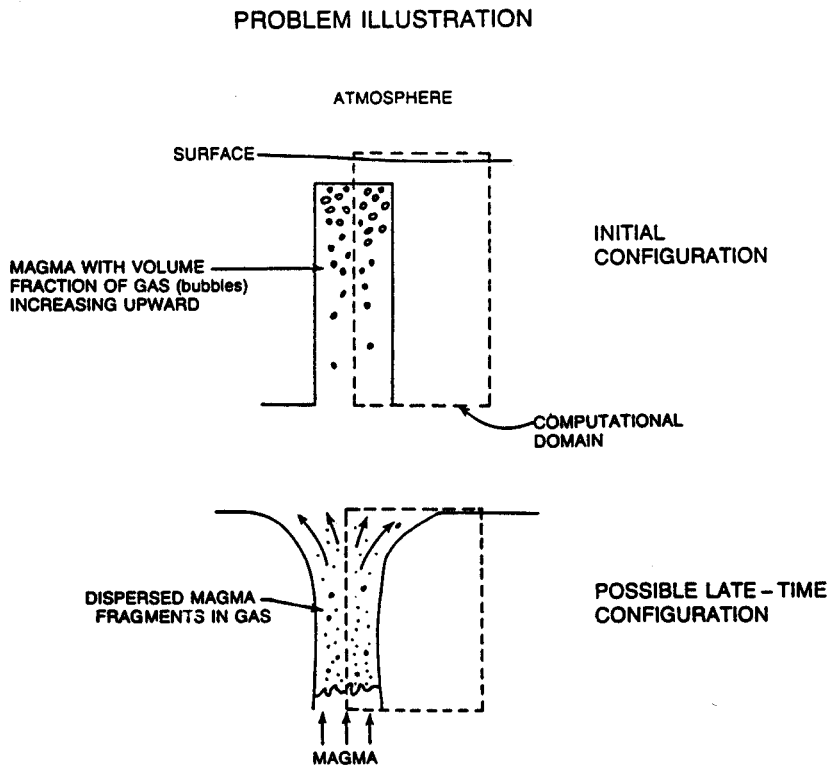

Figure 13. Sketch of the flow-field for multiphase flow in a lithospheric crack, which evolves into a flaring volcanic conduit

lithosphere in conduits. This research was initially followed in the KACHINA calculations of transient blast eruptions described above (Figure 6). It requires more detailed work to fully constrain the range of possible exit parameters for steady eruption types. Included in our calculations are the tracking of the rarefaction wave down the conduit and the effects of volatile mass fraction and its phase change after exsolution from the magma. This wave is followed by a fragmentation surface where the gas phase becomes continuous. Also, we calculate the effect of flow shear stress upon deformable and erodible conduit walls. Such processes can add country rock fragments to the flow. Figure 13 is a sketch of the relevant flow-field geometry.

A natural extension of the flow calculations in lithospheric conduits is a study of source 'triggers' for volcanic tremor. Chouet (1986) describes the frequency content of volcanic tremors by modeling seismic waves that radiate from a fluid-filled crack in the lithosphere. Although the crack need not be connected to a volcanic conduit, there is certainly the possibility that such a crack represents part of a conduit system. The coupling of wave propagation in the fluid with elastic waves in the crack walls is non-linear and results in a very slow wave called the 'crack wave' by Chouet (1986). The source disturbance in the fluid is not known, but preliminary consideration of the two-phase flow of a bubbly fluid and the growth and collapse of vapor bubbles in the fluid suggest that they are strong candidates for such a source trigger. This possibility is being investigated as a part of the conduit flow calculations.

Summary

We have applied the separated, two-phase hydrodynamic equations, including all important physical parameters, to modeling explosive volcanic eruptions. Two main types of eruption flow regimes are modeled: (i) unsteady, blast-type flows that involve highly transient effects, such as shock/rarefaction propagations and reflections

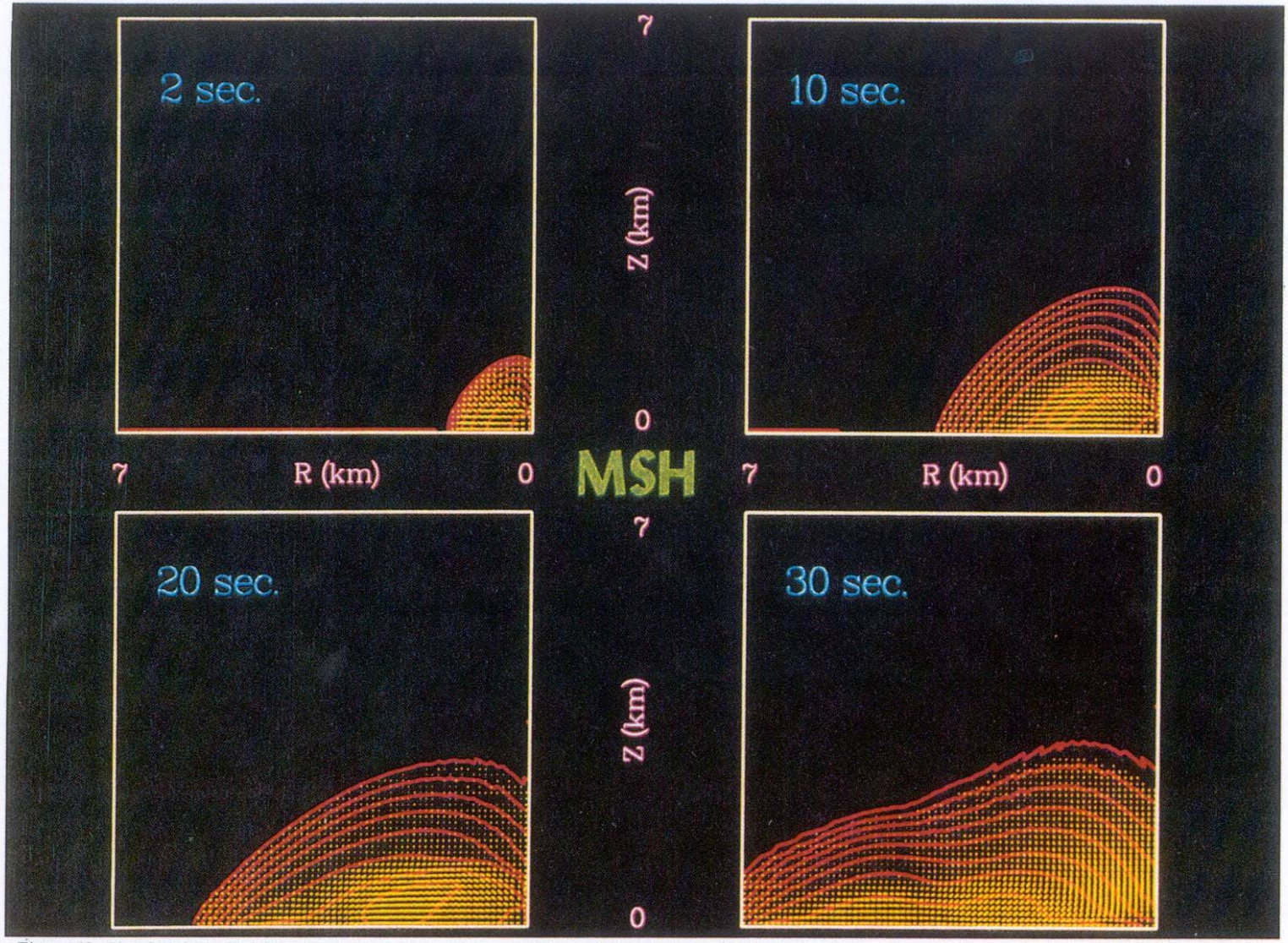

Figure 12. Simulated results of the blast phase of the 18 May, 1980 eruption of Mount St Helens using eruptive conditions of Kieffer (1981). The plots show overlays of ash velocity vectors (v_s) and contours of the logarithm of ash volume concentration [$\log(\theta_s)$]. These plots represent the blast during its evolution at 2, 10, 20 and 30 s, as if it were viewed looking east with the vent located in the lower right-hand corner of the plots. A Mach disk shock is inferred from pressure and density data to be located at a region about half way along the horizontal axis

and time-dependent flow within the volcanic conduit; and (ii) steady discharge eruptions in which vent exit conditions determine whether a high standing, buoyant plume or a collapsing negatively buoyant fountain are produced. The latter leads to the development of pyroclastic flows. In support of our calculations, we have recently successfully reproduced some of the characteristics of the Mount St Helens 18 May 1980 eruptions (Valentine and Wohletz, 1989b) and have early time (< 20 s) calculations that qualitatively support Kieffer's (1981) jet model for the blast phase of that eruption. It is interesting to note that both vertical and lateral jet orientations produce laterally moving pyroclastic surges, which suggests that the presence of solid particles in supersonic jets plays an important role in conversion of thermodynamic to kinetic energy. Such gravitational effects have traditionally hampered application of classical compressible fluid dynamics to dust-laden gases.

The numerical simulations are, in essence, 'numerical experiments' where the boundary and initial conditions are set by the operator with the results evolving continuously through time. These experiments can provide much insight into various related field observations, both of the activity of explosive eruptions and the tephra deposits that result. One example of this type of experimental observation is the pyroclastic flow erosion and depositional history mentioned above. Other examples include the flow dynamics that lead to depositional facies of pyroclastic flows, such as proximal coignimbrite breccias, the ground surge that is commonly found at the base of pyroclastic flow deposits, the ash-cloud surge that is in many places deposited over pyroclastic flows, and the lateral depositional facies, determined by both tephra size and volume concentration. The simulations can also aid in the interpretation of active eruption behavior. For example, simulations show that the ash plume, convectively rising above a fountain, can reach upward speeds much greater than the actual exit velocity at the vent, and that pyroclastic flow runout is affected by eruption-induced atmospheric convection (Valentine and Wohletz, 1989b). Although numerical simulations can never completely substitute for observations of the natural processes, *they do have the advantage that one can see inside the flow*, whereas in nature most of the important processes are hidden by veils of ash. Numerical simulations cannot stand alone of course, but they are absolutely necessary for an insightful understanding of most field observations of explosive volcanic activity.

An important lesson learned from studying the multiphase hydrodynamics of explosive eruptions is that a rich complexity of processes is predicted by the relatively straightforward set of governing equations (equations (1) through (6)). This diversity is the result of the inherent, non-linear nature of these equations; small changes in the parameters may produce very different solutions. This complexity thus suggests that for a given field observation, there may be several equally plausible physical explanations. Therefore extreme caution should be taken in the interpretation of field observations, such as the comparison of several different eruptions, even at the same volcano.

There are numerous directions that can be followed in future computer studies of explosive eruptions. One of these, the flow within volcanic conduits through the lithosphere, is of current interest. Eventually, we will combine the conduit and external flow-fields into one calculation, using a variable mesh size and time-step. We have heretofore constrained our calculations to single particle sizes and, because the effect of multiple sizes is non-linear, we have not attempted to superimpose solutions for simulations of different sizes. However, Horn (1989) has developed the DANIEL code at Los Alamos to calculate the effects and trajectories of particles of various sizes and densities in a multiphase hydrodynamic calculation. Additional collaboration with Susan W. Kieffer of the US Geological Survey will involve the study of the detailed physics of the atmospheric flow-field in a search for flow singularities and the effects of high particle concentrations, topographic barriers, and various column (jet) orientations.

Acknowledgements

We thank Eric Jones, Brook Sandford, Marty Horn, and Rod Whitaker for the years of support they have given in the development and application of computer codes to geologic problems and especially their unique insight into the physics of dynamic processes. Frank Harlow has been a great teacher of the methods of computational

fluid dynamics, and he has encouraged and challenged us to build further and improve on his work. Alan P. Boss and Lionel Wilson provided helpful reviews. Finally, Chick Keller, Sumner Barr, and Wes Myers have been instrumental in providing administrative support for this work. This work has been done under the auspices of the US Department of Energy through the Office of Basic Energy Science and Institutional Supporting Research and Development at Los Alamos National Laboratory.

References

Besnard, D.C. and Harlow, F.H. (1988). Turbulence in multiphase flow. *Int. J. Multiphase Flow*, **14**, 679–699.

Carey, S. and Sigurdsson, H. (1985). The May 18 1980 eruption of Mount St Helens; 2. Modeling of dynamics of the Plinian phase. *J. Geophys. Res.*, **90**, 2948–2958.

Chouet, B. (1986). Dynamics of a fluid-driven crack in three dimensions by the finite difference method. *J. Geophys. Res.*, **91**, 13967–13992.

Courant, R. and Friedrichs, K.P. (1948). Supersonic flow and shock waves. Interscience, New York, 464 pp.

Ferziger, J.H. (1981). *Numerical Methods for Engineering Applications*. Wiley, New York, 270 pp.

Glasstone, S. and Dolan, P.J. (1977). *The Effects of Nuclear Weapons*. US Department of Defense and US Department of Energy, Washington, DC, 653 pp.

Harlow, F.H. and Amsden, A.A. (1975). Numerical calculation of multiphase fluid flow. *J. Comput. Phys.*, **17**, 19–52.

Hildreth, W. (1979). The Bishop Tuff: evidence for the origin of compositional zonation in silicic magma chambers. *Geol. Soc. Am. Spec. Pap.*, **180**, 43–75.

Hirt, C.W. (1968). Heuristic stability theory for finite-difference equations. *J. Comput. Phys.*, **2**, 339–355.

Horn, M. (1986). *Physical models of pyroclastic clouds and fountains*, MS Thesis, Arizona State University, Tempe, 125 pp.

Horn, M. (1989). *A Computer Code for High-speed Dusty Gas Flows with Multiple Particle Sizes*. Los Alamos National Laboratory, Los Alamos, NM, LA-11445-MS, 59 pp.

Hunter, J.H., Sandford II, M.T., Whitaker, R.W., and Klein, R.I. (1986). Star formation in colliding gas flows. *Astrophys. J.*, **305**, 309–332.

Ishii, M. (1975). *Thermo-fluid Dynamic Theory of Two-phase Flow*. Collection de la Direction des Etudes et Recherches d'Electricite de France, Eyrolles, Paris, 200 pp.

Kieffer, S.W. (1981). Fluid dynamics of the May 18 Blast at Mount St Helens. In: Lipman, P.W. and Mullineaux, D.R. (eds) *The 1980 Eruptions of Mount St Helens, Washington*. US Geol. Surv. Prof. Pap. 1250, pp. 379–400.

Kieffer, S.W. (1982). Dynamics and thermodynamics of volcanic eruptions: Implications for the plumes on Io. In: Morrison, D. (ed.) *Satellites of Jupiter*. University of Arizona Press, Tucson, pp. 647–723.

Kieffer, S.W. (1984). Factors governing the structure of volcanic jets. In: Boyd, F.R. (ed.) *Explosive Volcanism: Inception, Evolution, and Hazards*. National Academy Press, Washington, DC, pp. 143–157.

Kieffer, S.W. and Sturtevant, B. (1984). Laboratory studies of volcanic jets. *J. Geophys. Res.*, **89**, 8253–8268.

MacDonald, G.A. (1972). *Volcanoes*, Prentice-Hall, Englewood Cliffs, NJ, 510 pp.

Mercali, G. and Silvestri, D. (1891). Le eruzioni dell'isola di Vulcano, incominciate il 3 Agosta 1888 e terminate il 22 Marzo 1890: Relazione scientifica 1891. *Ann. Uff. Centr. Meterol. Geodent.*, **10**(4), 135–148.

Shapiro, A.H. (1953). *The Dynamics and Thermodynamics of Compressible Fluid Flow*, Vol. I. Wiley, New York, 647 pp.

Smith, R.L. (1979). Ash flow magmatism. *Geol. Soc. Am. Spec. Pap.*, **180**, 5–27.

Sparks, R.S.J., Wilson, L., and Hulme, G. (1978). Theoretical modeling of the generation, movement, and emplacement of pyroclastic flows by column collapse. *J. Geophys. Res.*, **83**, 1727–1739.

Travis, J.R., Harlow, F.H., and Amsden, A.A. (1975). *Numerical Calculation of Two-phase Flows*. Los Alamos National Laboratory, Los Alamos, NM, LA-5942-MS, 20 pp.

Ulam, S. (1980). Von Neumann: the interaction of mathematics and computing. In: Metropolis, N., Howlett, J. and Rota, G.-C. (eds) *A History of Computing in the Twentieth Century*. Academic Press, New York, pp. 93–99.

Valentine, G.A. and Wohletz, K.H. (1989a). Numerical models of plinian eruption columns and pyroclastic flows. *J. Geophys. Res.*, **94**, 1867–1887.

Valentine, G.A. and Wohletz, K.H. (1989b). Environmental hazards of pyroclastic flows determined by numerical models. *Geology*, **17**, 641–644.

Von Neumann, J. and Richtmyer, R.D. (1949). A method for the numerical calculation of hydrodynamic shocks. *J. Appl. Phys.*, **21**, 232–238.

Walker, G.P.L. (1973). Explosive eruptions—a new classification scheme. *Geol. Rundsch.*, **62**, 431–446.

Walker, G.P.L. (1981). Plinian eruptions and their products. *Bull. Volcanol.*, **44**, 223–240.

Wilson, L. (1980). Relationships between pressure, volatile content and ejecta velocity in three types of volcanic explosion. *J. Volcanol. Geotherm. Res.*, **8**, 297–313.

Wilson, L., Sparks, R.S.J., and Walker, G.P.L. (1980). Explosive volcanic eruptions, IV. The control of magma properties and conduit geometry on eruption column behavior. *Geophys. J. R. Astron. Soc.*, **63**, 117–148.

Wohletz, K.H., McGetchin, T.R., Sandford II, M.T., and Jones, E.M. (1984). Hydrodynamic aspects of caldera-forming eruptions: numerical models. *J. Geophys. Res.*, **89**, 8269–8285.

Woods, A.W. (1988). The fluid dynamics and thermodynamics of eruption columns. *Bull. Volcanol.*, **50**, 169–193.

Wright, J.K. (1967). *Shock Tubes*. Methuen, London, 100 pp.